Journal of Mechatronics Engineering

EFFECTS OF La_2O_3 AND Bi_2O_3 ADDITIONS ON THE MICROWAVE DIELECTRIC AND ANTENNA PROPERTIES OF $SrBi_2Nb_2O_9$ CERAMIC MATRIX

ROTERDAN FERNANDES ABREU[1,2], FELIPE RODRIGUES DA SILVA[4], SAMUEL OLIVEIRA SATURNO[1,2], DIEGO DA MOTA COLARES[1,2], TALLISON OLIVEIRA ABREU[2,3], JOÃO PAULO COSTA DO NASCIMENTO[2,4], EMMANUELLE DE OLIVEIRA SANCHO[5], JUSCELINO CHAVES SALES[6], DANIEL XAVIER GOUVEIA[2,4], ANTONIO SÉRGIO BEZERRA SOMBRA[1,2,7],

[1] Telecommunication Engineering Department, Federal University of Ceará (UFC), Fortaleza, Ceará, 60755-640, Brazil;
[2] Physics Department - Federal University of Ceará (UFC), LOCEM-Telecommunication and Materials Science and Engineering of Laboratory (LOCEM), Campus PICI, P.O. Box 6030, Fortaleza, Ceará, 60455-760, Brazil; <roterdan.fernandes@gmail.com>, <samuel.saturno@alu.ufc.br>, <diegodamotacolares@gmail.com>
[3] Department of Organic and Inorganic Chemistry, Science Center, Federal University of Ceará (UFC), Brazil; <tallisabreu@gmail.com>
[4] Federal Institute of Education, Science and Technology of Ceará, PPGET, Fortaleza, Ceará, Brazil; <feliperodrigues199@hotmail.com>, <jpquimico3@gmail.com>, <dxgouveia@gmail.com>
[5] Departamento de Engenharia Mecânica, Universidade de Fortaleza - UNIFOR, Fortaleza, Ceará 60811-905, Brazil; <emmanuellesancho@hotmail.com>
[6] State University of Vale do Acaraú, Center for Exact Sciences and Technology, Department of Civil Engineering; <juscelinochaves@hotmail.com>
[7] Laboratory of Communication and Security Networks (LARCES), State University of Ceará, Itaperi Campus, Fortaleza, Ceará, Brazil. <asbsombra@gmail.com>

DOI: http://dx.doi.org/10.21439/jme.v4i2.94

Received: 25 May 2021. **Accepted:** 12 July 2021

Abstract. This work presents a comparison between the dielectric properties of the $SrBi_2Nb_2O_9$(SBN) ceramic matrix and the individual additions of Bi_2O_3 and La_2O_3, suggesting the material that would be most suitable for microwave applications. The SBN sample was synthesized by solid-state reaction, and the X-ray diffraction method (XRD) was used for the structural characterization of the materials analyzed in this study. Thermal stability of the samples was measured experimentally by studying the temperature coefficient of resonant frequency (τ_f) the results confirm that the individual additions of 15 wt% of Bi_2O_3 or La_2O_3 improved the thermostability of the composites. The Hakki-Coleman method was used to obtain the dielectric properties in the microwave range, and it is possible to observe that the dielectric permittivity of the composites increased, while their loss tangents decreased. The numerical simulation demonstrated the functioning of the materials as dielectric resonating antennas (DRA), with a reflection coefficient below -10 dB in all samples.

Keywords: $SrBi_2Nb_2O_9$. Microwave. Bi_2O_3. La_2O_3. DRA.

1 Introduction

Dielectric ceramics have notable importance to the global communications system due to applications ranging from cellular telephony to global positioning systems (GPS). Their high permittivity and low losses allow the miniaturization and use of these materials in different electronic components, such as filters, oscillators, amplifiers, tuners, etc. (ABREU et al., 2021; MOULSON; HERBERT, 2003; SEBASTIAN, 2008; WANG et al., 2020).

$SrBi_2Nb_2O_9$ (SBN) ceramic matrix is a ferroelectric with structured layers of bismuth, has an Aurivillius phase, consisting of alternating layers of $(SrNb_2O_2)^{2-}$ perovskite and $(Bi_2O_2)^{2+}$. (KUMAR et al., 2019; WEI et al., 2020; WU, 2018) . Ferroelectric materials have high permissiveness values, good piezoelectric coefficients, and spontaneous polarization, which make these materials suitable for many technological applications. In addition, these materials have high resistance to fatigue and their potential use in random access memories has been constantly investigated (SANCHO et al., 2013; SINGH et al., 2018; WU et al., 2017). Recent studies show the possibility of application as dielectric resonator antennas (DRA) of the SBN matrix with additions of Bi_2O_3 or La_2O_3 (ABREU et al., 2019; ABREU et al., 2020).

The objective of this work was to compare the influence of individual additions of 15 wt% of La_2O_3 or Bi_2O_3 on ceramic matrix $SrBi_2Nb_2O_9$ (SBN), showing the influence of these additions on the dielectric characteristics of this ceramic material and the possibility of applications in microwave devices (MW) of materials investigated. The effect of additions of the SBN pure phase on structural identification and its dielectric properties in the microwave range were analyzed. X-ray diffraction (XRD) was used for the structural characterization of the samples, and the confirmation of the phases was obtained through the Rietveld refinement (ABREU et al., 2021; NASCIMENTO et al., 2020; RIETVELD, 1969). Dielectric properties in the microwave region were studied using the Hakki-Coleman method (COURTNEY, 1970; HAKKI; COLEMAN, 1960), and through the technique developed by Long, Macllister, and Shen (LONG; MCALLISTER; SHEN, 1983; MCALLISTER; LONG; CONWAY, 1983). Thermal stability of the material was investigated using the Silva-Fernandes-Sombra (SFS) method (SILVA; FERNANDES; SOMBRA, 2012). Numerical simulation was carried out to obtain the far-field parameters and, in this way, to compare the behavior of the materials as a dielectric resonant antenna (DRA).

2 Materials and Methods

Samples were prepared through the conventional ceramic method. The precursor oxides $SrCO_3$, Bi_2O_3, Nb_2O_5 were ground for 8 h at 360 rpm using the Fritsch Pulverisette 5 mill, and calcined in a JUNG resistive oven (LF0912) at 900ºC for 2h. After this process, 15 wt% of Bi_2O_3 or 15wt% of La_2O_3 was added on SBN, resulting in samples SBNBi and SBNLa. Samples were compacted via uniaxial pressure of 294 MPa in the bulk format using 5% glycerin as a binder and were sintered in the conventional controlled furnace (JUNG - LF0912), respectively, at 900ºC / 2h, 850ºC / 2h, and 1000ºC / 2h.

Structural analysis of the samples was performed using X-ray diffraction (XRD), and the phases were identified using the X´Pert HighScore Plus program and the Inorganic Crystal Structure Database (ICSD).

Through the Hakki – Coleman method (COURTNEY, 1970; HAKKI; COLEMAN, 1960), and using the HP8716ET network analyzer from Hewllet - Packard (HP), the dielectric properties of the samples were obtained. The analysis of the sample's characteristic spectrum determines the resonance modes of the resonator, which allowed to calculate dielectric permittivity (ε_r), dielectric loss tangent (tan δ) and quality factor (Q = 1 / tanδ) of the compounds analyzed.

To analyze the thermal stability of the materials, the Silva-Fernandes-Sombra (SFS) method was employed. This method analyzes the dominant mode and τ_f an be calculated analytically using equation (1) (SILVA; FERNANDES; SOMBRA, 2012):

$$\tau_f = \frac{1}{f_0} \cdot \frac{\Delta f}{\Delta T} \cdot 10^6 \; ppm/^\circ C \qquad (1)$$

Where $f0$ is the resonance frequency at the beginning of the process, Δf the difference between the final and initial frequencies, and ΔT the difference between the final and initial temperatures.

For the performance of the dielectric resonator antenna (DRA) was employed the technique developed by Long, Mcallister, and Shen using Agilent Network Analyzer N5230A network. The samples are excited under the DRA configuration (Fig. 1), the probe (d = 9.6 mm) is connected to the ground plane made of copper (35.5 cm x 30 cm x 2.14 mm). The cylindrical DRA

has a radius (a), height (h), and (d) is the height of the probe.

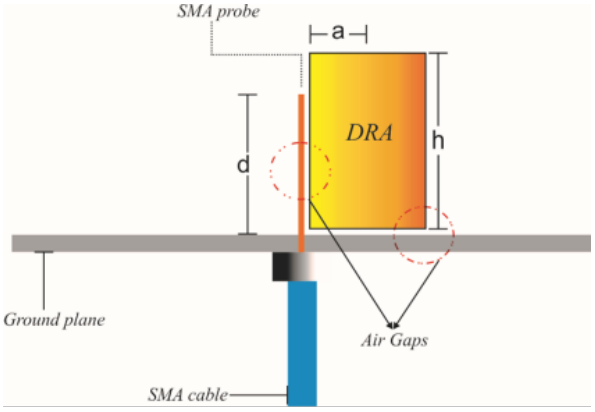

Figure 1: Setup for the DRA measurement

According to the literature (ABREU et al., 2021; ABREU et al., 2021), the quality factor Q and the resonant frequency can be accurately calculated according to the following equations,

$$Q_{(HE_{11\tau})} = 0.01007(\varepsilon_r^{1.3}) \cdot \frac{a}{h}\left[1 + 100e^{-2.05\left(\frac{a}{2h} - 0.0125\left(\frac{a}{h}\right)^2\right)}\right] \quad (2)$$

and,

$$f_{(HE_{11\tau})} = \frac{6.324c}{2\pi a\sqrt{\varepsilon_r + 2}}\left[0.27 + 0.36\left(\frac{a}{2h}\right) + 0.02\left(\frac{a}{2h}\right)^2\right] \quad (3)$$

From the experimental results of return loss (S11) and the real (Z') and imaginary (Z") impedances, a numerical simulation was carried out to obtain far-field parameters, compare experimental results with simulated ones and, evaluate the application of materials such as DRA (HAYDOURA et al., 2021; OLIVEIRA et al., 2019). Ansoft HFSS® (High-Frequency Structure Simulator) software was used to perform the simulation and through it was possible to obtain the parameters: directivity, gain, antenna efficiency, and radiation diagram, etc (ABREU et al., 2021).

3 Results and discussion

SBN, SBNBi, and SBNLa phases were analyzed through X-ray diffraction. The diffractogram of the SBNBi, when compared to the SBN matrix (Fig. 2a), demonstrates the formation of a new phase that was identified as $(Sr_{0.6}Bi_{0.3}0_5)_2Bi_2O_7$ (JCPDS 73-923). For SBNLa samples (Fig. 2b) was observed the presence of $LaNbO_4$ (JCPDS nº. 81-618) as a secondary phase. When the added samples are compared to the SBN sample without addition, no significant shift in the peak positions was observed in the pure sample indicating that its crystalline structure was not affected by the additions.

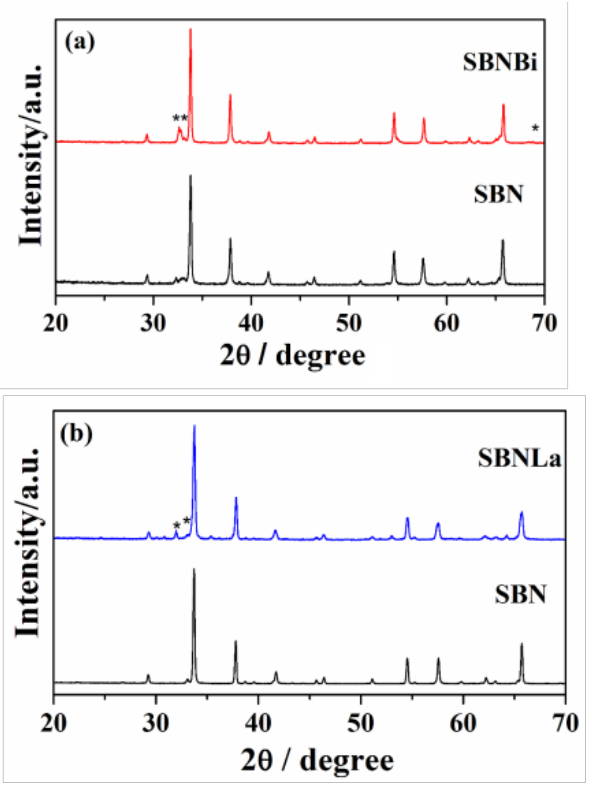

Figure 2: X-ray diffraction of SBN samples, (a) SBNBi and ♦ Bi_3NbO_7, (b) SBNLa, * $LaNbO_4$.

In Fig. 3 a-c are shown results obtained by the Rietveld refinement of the samples, where SBN and $(Sr_{0.6}Bi_{0.3}0_5)_2Bi_2O_7$ phases were used in the refinement of the SBNBi, while SBN and $LaNbO_4$ were used to the refinement of the SBNLa. The low residual values between the observed and calculated diffraction patterns indicate that the refinement performed is reliable. The lattice parameters, convergence indexes Rwp (weighted residual error), Rexp (value expected for Rwp) and S (goodness of fit), where S is given by the Rwp / Rexp ratio, are shown in Table 1.

Through the Hakki – Coleman method (COURTNEY, 1970; HAKKI; COLEMAN, 1960), the dielectric properties ε_r, tan δ, and Q_d x f_r were obtained, and the results are shown in Table 2. Comparing the samples

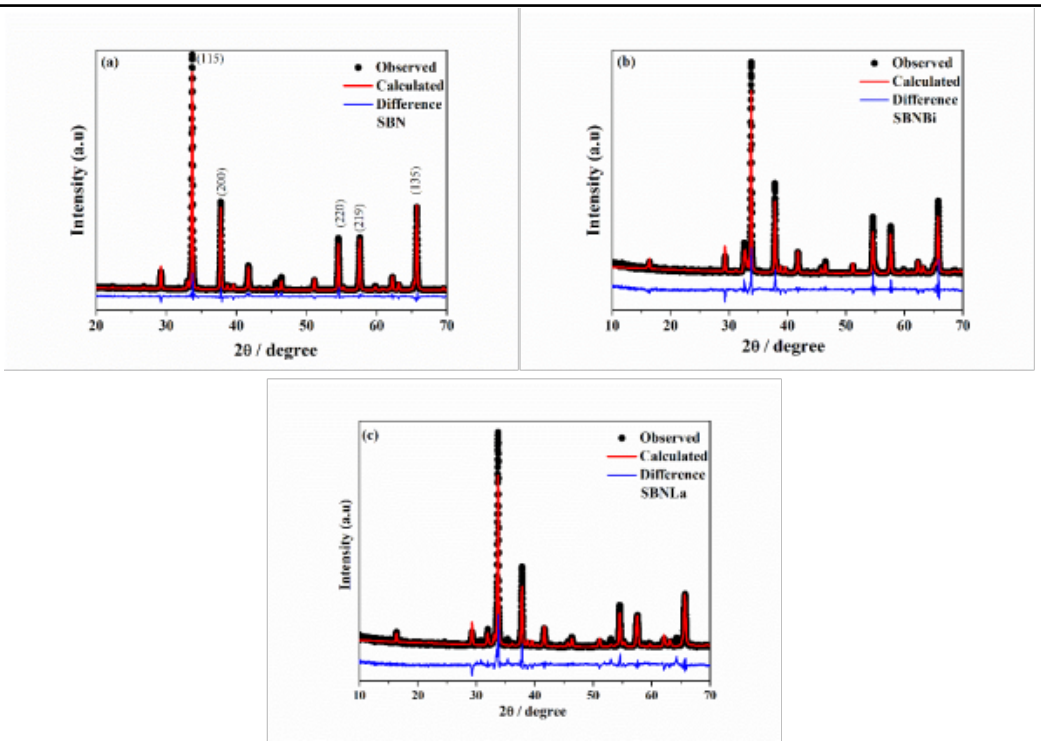

Figure 3: Rietveld refinement of samples from (a) SBN, (b) SBNBi, and (c) SBNLa.

Table 1: Parameters obtained in the Rietveld Refinement for SBN samples.

Samples	R-P (%)	R-WP (%)	S (%)	D-WP
SBN	12.43	17.19	1.90	0.13
SBNBi	17.43	22.07	1.61	0.06
SBNLa	17.78	22.76	1.75	0.05

added with the pure SBN, it was possible to notice that additions caused a decrease in the tangent of losses (tan δ), and the increase in electrical permittivity (ε_r) and the quality factor Q_d. The highest permissiveness (ε_r = 104.82) and the lowest loss tangent (tan δ = 0.0186) were found for the SBNBi.

SBN pure phase presented a τ_f = -345.62 ppm/ºC, this fact was the initial motivation for the addition of oxides Bi_2O_3 or La_2O_3, due to the possibility of obtaining new composites with higher thermal stability and better dielectric properties. SBNBi sample demonstrated τ_f = -235.02 ppm/ºC and SBNLa presented τ_f = -116.51 ppm/ºC, value closer to zero for addition with La_2O_3 could be explained by the formation of the $LaNbO_4$ phase that has positive τ_f (KIM et al., 2006). These results are extremely important for microwave applications, as they demonstrate an increase in the thermal stability of the SBN matrix and they encourage the manufacture of new composites with greater additions. Analyzing the results obtained, it is observed that the additions made in the SBN matrix caused the improvement of the main properties necessary for a DRA (ABREU et al., 2021; HAYDOURA et al., 2021; PETOSA, 2007).

Far-field parameters were obtained through numerical simulation using the Ansoft HFSS® software, these data provide the operation standards of the materials such as DRA. In the simulation performed, the experimental and simulated results for return loss (S_{11}), Z', Z" and the Smith Chart were compared. In Fig. 4 it is possible to observe the excellent fit between the experimental and simulated profile.

According to Table 3 and Fig. 4, it can be noted that all samples showed a return loss with values well below -10 dB, a value required for applications such as DRA (BALANIS, 2011). Return loss (S11) indicates the loss of energy due to discontinuity in the transmission line/device, that is, the more negative this parameter is, the less energy is lost (POOLE; DARWAZEH, 2015). It is worth mentioning that the error between the

Table 2: Microwave measurements of materials using the Hakki-Coleman method.

Sample	D (mm)	H (mm)	ε_r	tan δ (10^{-2})	Q_d x f_r (GHz)	τ_f (ppm/ºC)
SBN	17.78	8.96	28.6	3.24	135.37	-345.62
SBNBi	15.02	7.88	104.82	1.86	142.63	-235.02
SBNLa	16.94	8.40	23.54	1.87	273.44	-116.51

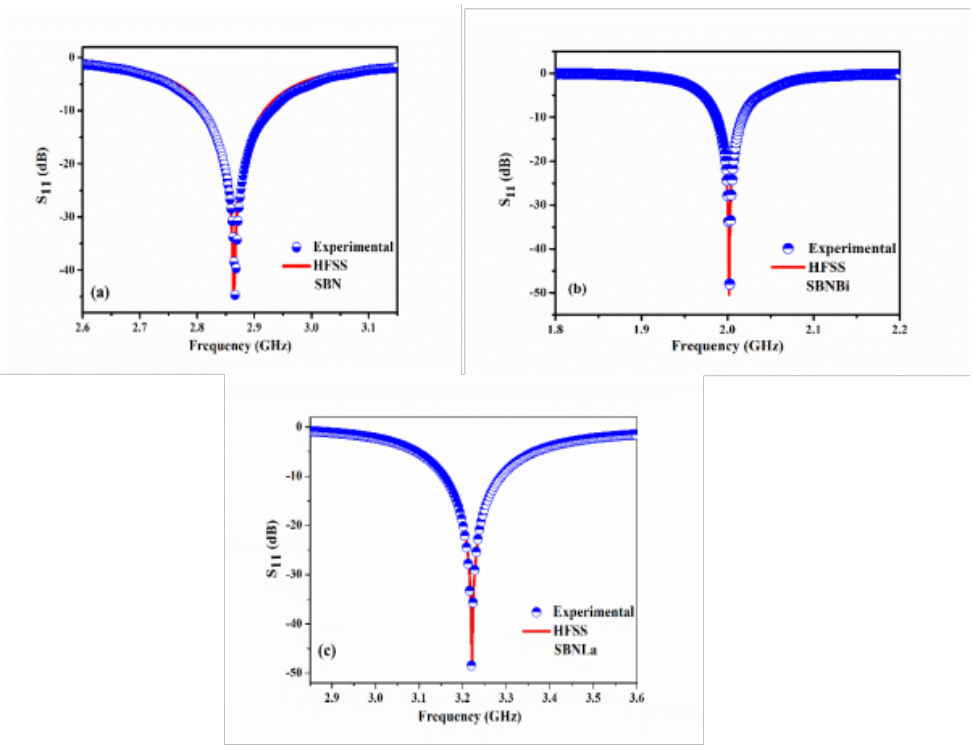

Figure 4: Return loss (S11) of the samples (a) SBN, (b) SBNBi, (c) SBNLa.

simulated frequency and the measurement is practically zero for all samples, as can be seen in Table.

Table 3: Frequency and return loss (S_{11}) experimental and simulated for the $HE_{11\delta}$ resonant mode.

	f_r (GHz)			S_{11} (dB)		
Sample	**Exp**	**Sim**	**Error (%)**	**Exp**	**Sim**	**Error (%)**
SBN	2.86	2.86	0.00	-49.97	-45.01	0.08
SBNBi	2.86	2.86	0.00	-49.67	-48.03	3.41
SBNLa	3.22	3.21	0.06	-48.58	-48.49	0.22

Fig. 5 shows the experimental and simulated diagrams of the real Z' (Ω) and imaginary Z"(Ω) of the complex impedance. It is possible to notice that all samples showed a good agreement indicating that the simulation performed was adequate.

Fig. 6 shows Smith Chart for the three samples analyzed in this study. It is possible to perceive an inductive character in SBN and SBNLa since its semi-circular regions are displaced upwards from the horizontal axis, while the SBNBi sample has a more capacitive character since its semi-circular regions are more displaced downwards horizontal axis (POOLE; DARWAZEH, 2015).

With the data obtained from the monopole experiment and using numerical simulation, it was possible to obtain the following far-field parameters: Directivity; Gain; Reflection coefficient (Γ); Voltage standing wave ratio (VSWR); Energy reflection coefficient (Γ_{pwr}); Energy transmission coefficient (T_{pwr}); Radiation efficiency (Eff). It is worth mentioning that these data provide the operation standards of materials such as DRA or other devices that operate in the microwave region (ABREU et al., 2021; POOLE; DARWAZEH, 2015).

Data from Table 4 demonstrate that the VSWR of all samples is very close to 1, indicating that a good part of the energy is being transmitted and little is lost by reflection. The energy transmission coefficient (T_{pwr}) indicates how much power is transmitted as a function of the incompatibility in the transmission line (POOLE; DARWAZEH, 2015), that is, the closer to 1 this value, the greater the energy transmission and the lower the loss due to impedance mismatch and all samples meet this requirement. The energy reflection coefficient (Γ_{pwr}) indicates how much energy is lost by reflection, the closer to zero this parameter is, the less energy is lost, and all samples have a value in the range of 10^{-5}. Finally, the radiation efficiency of the three samples was calculated, with the best efficiency being observed for the SBNLa sample (Eff = 80.63%). The resonant frequency of the materials is in the range of 2 - 4 GHz allowing them to act as devices that operate in the S-band according to the classification from IEEE (BALANIS, 2012; CHANG, 2000; POOLE; DARWAZEH, 2015; POZAR, 2012; STUTZMAN; THIELE, 2012). The results obtained demonstrate that the simulation carried out suggests potential applications for the SBNBi and SBNLa phases as DRA's or in other devices that operate in the microwave range, such as microwave filters, oscillators, radar detectors, etc.

4 Conclusion

In this work, we have analyzed the effects of individual additions of Bi_2O_3 or La_2O_3 on $SrBi_2Nb_2O_9$ (SBN) ceramic matrix, comparing their dielectric properties as well as the performance of these materials as DRA. The structural analysis of the SBN matrix and additions was performed through X-ray diffraction (XRD), and the Rietveld refinement confirmed the presence of SBN, as well as the formation of secondary phases in the added samples. The analysis of the dielectric properties demonstrated that the additions caused the reduction of tan δ and the increase of ε_r, in addition to causing an increase in the thermal stability of the SBN matrix.

Numerical simulation showed that all samples showed loss of return below -10 dB and operated in the region of the S-band (2 - 4 GHz), making them potential candidates for use in communication satellites and radars, and the results of the far-field parameters demonstrated that SBNLa demonstrated to be the most efficient material for application as DRA, since it presented higher values of directivity, gain and radiation efficiency.

ACKNOWLEDGMENTS

This work was partly sponsored by the Brazilian Research Agencies CNPq-Conselho Nacional de Desenvolvimento Científico e Tecnológico (grant INCT NANO(BIO)SIMES), CAPES- Coordenação de Aperfeiçoamento de Pessoal de Ensino Superior (grant Project PNPD), FINEP-Financiadora de Estudos e Projetos (grants INFRAPESQ-11 and INFRAPESQ-12), and the U. S. Air Force Office of Scientific Research (AFOSR) (FA9550-16-1-0127).

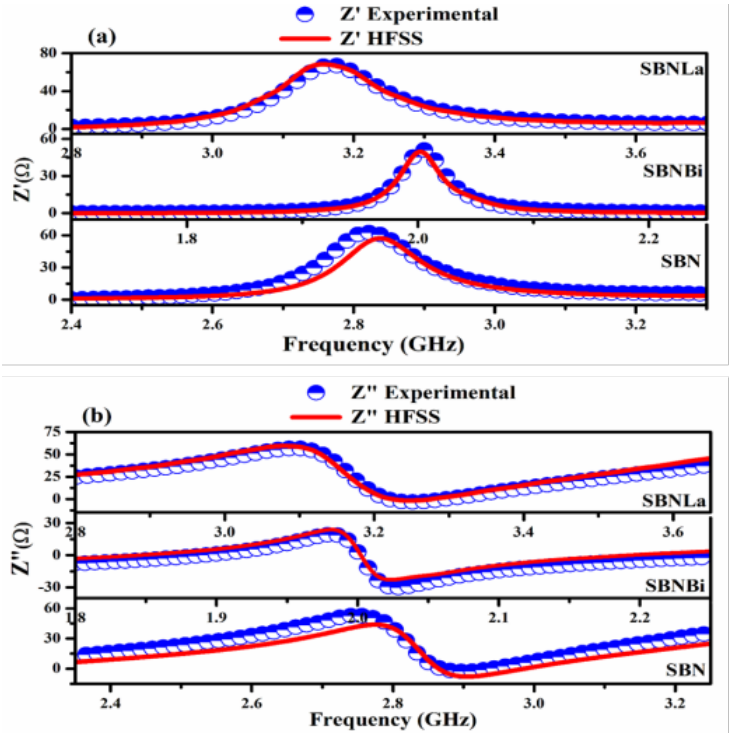

Figure 5: Experimental and simulated diagrams of the complex impedance (a) real part Z '(Ω) (b) imaginary part Z "(Ω).

Table 4: Directivity; Gain; Reflection coefficient (Γ); Voltage standing wave ratio (VSWR); Energy reflection coefficient (Γ_{pwr}); Energy transmission coefficient (T_{pwr}); Efficiency of radiation (Eff); Determined by the simulation in the HFSS.

Sample	**Direc. (dBi)**	**Gain (dBi)**	Γ	**VSWR**	Γ_{pwr}	$\mathbf{T}_{pwr}$	**Eff. (%)**
SBN	6.62	5.56	0.003173	1.00636	0.00001	0.9999	78.19
SBNBi	6.90	3.11	0.003284	1.00659	0.00001	0.9999	41.85
SBNLa	6.92	5.98	0.003723	1.00747	0.00001	0.9999	80.63

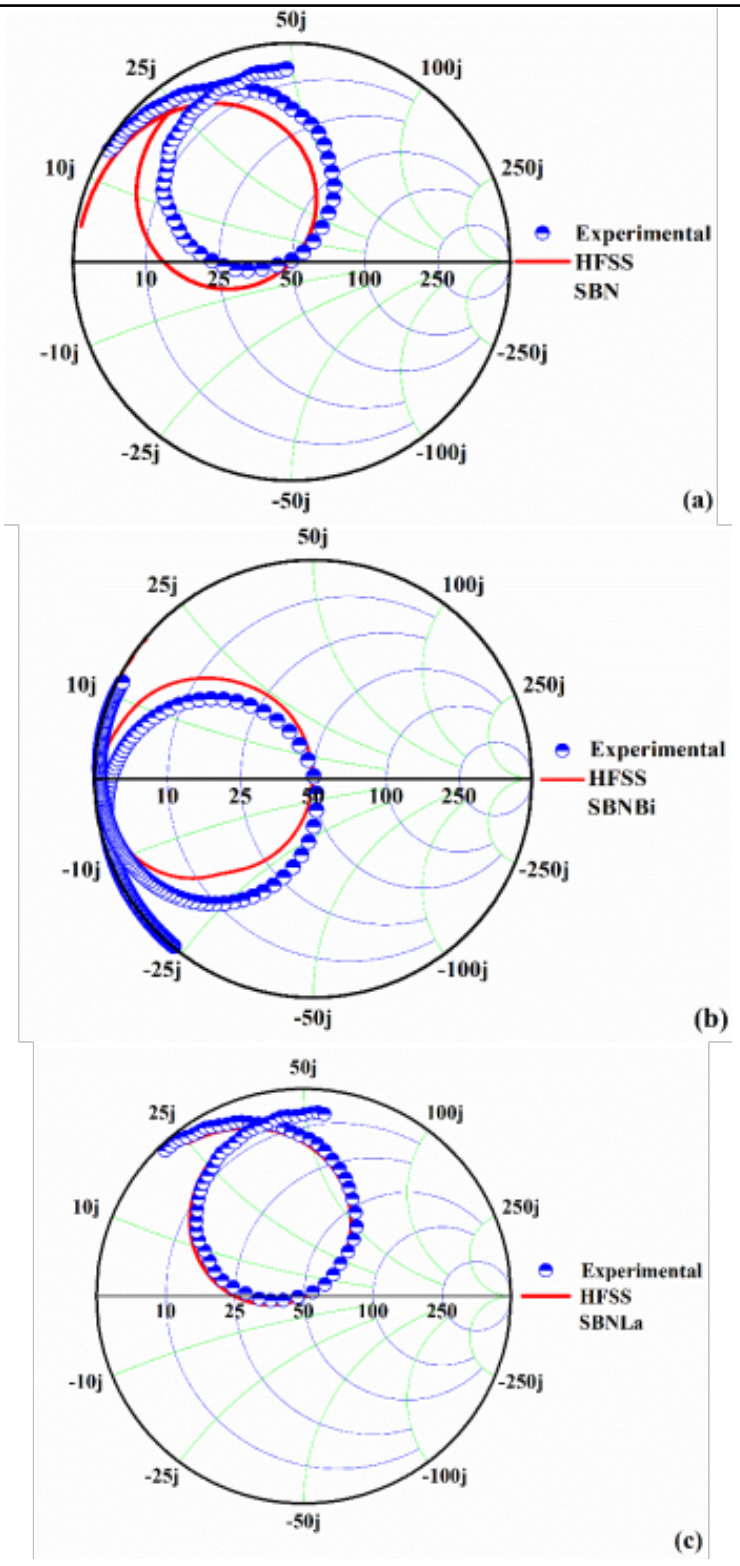

Figure 6: Smith charts experimental and simulated from: (a) SBN, (b) SBNB andi (c) SBNLa.

References

ABREU, R.; ABREU, T.; COLARES, D. d. M.; SATURNO, S.; NASCIMENTO, J. do; NOBREGA, F.; GHOSH, A.; VASCONCELOS, S.; SALES, J.; ANDRADE, H. de et al. Evaluation of dielectric properties of the barium titanium silicate (ba 2 tisi 2 o 8) for microwave applications. **Journal of Materials Science: Materials in Electronics**, Springer, v. 32, n. 6, p. 7034–7048, 2021.

ABREU, R.; SATURNO, S.; NASCIMENTO, J. do; SANCHO, E.; MORAIS, J. de; SALES, J.; GOUVEIA, D.; ANDRADE, H. de; JÚNIOR, I. Q.; SOMBRA, A. Dielectric characterisation and numerical investigation of srbi2nb2o9–bi2o3 composites for applications in microwave range. **Journal of Electromagnetic Waves and Applications**, Taylor & Francis, v. 34, n. 12, p. 1705–1718, 2020.

ABREU, R.; SATURNO, S.; SANCHO, E.; GOUVEIA, D.; SOMBRA, A. Microwave dielectric properties study of the la 2 o 3 additions on the srbi 2 nb 2 o 9 matrix. **Journal of Electronic Materials**, Springer, v. 48, n. 2, p. 1196–1206, 2019.

ABREU, T. O.; ABREU, R. F.; CARMO, F. F. do; SOUSA, W. V. de; BARROS, H. d. O.; MORAIS, J. E. de; NASCIMENTO, J. P. do; SILVA, M. A. da; TRUKHANOV, S.; TRUKHANOV, A. et al. A novel ceramic matrix composite based on ynbo4–tio2 for microwave applications. **Ceramics International**, Elsevier, v. 47, n. 11, p. 15424–15432, 2021.

BALANIS, C. A. **Modern Antenna Handbook**. [S.l.], 2011.

____. **Antenna Theory: Analysis and Design**. [S.l.], 2012. Vol. 28.

CHANG, K. **RF and microwave wireless systems**. 1. ed. New York, USA: John Wiley & Sons, 2000.

COURTNEY, W. E. Analysis and evaluation of a method of measuring the complex permittivity and permeability microwave insulators. **IEEE Transactions on Microwave Theory and Techniques**, IEEE, v. 18, n. 8, p. 476–485, 1970.

HAKKI, B.; COLEMAN, P. D. A dielectric resonator method of measuring inductive capacities in the millimeter range. **IRE Transactions on Microwave Theory and Techniques**, IEEE, v. 8, n. 4, p. 402–410, 1960.

HAYDOURA, M.; BENZERGA, R.; PAVEN, C. L.; GENDRE, L. L.; LAUR, V.; CHEVALIER, A.; SHARAIHA, A.; TESSIER, F.; CHEVIRÉ, F. Perovskite (sr2ta2o7) 100- x (la2ti2o7) x ceramics: From dielectric characterization to dielectric resonator antenna applications. **Journal of Alloys and Compounds**, Elsevier, v. 872, p. 159728, 2021.

KIM, D.-W.; KWON, D.-K.; YOON, S. H.; HONG, K. S. Microwave dielectric properties of rare-earth ortho-niobates with ferroelasticity. **Journal of the American Ceramic Society**, Wiley Online Library, v. 89, n. 12, p. 3861–3864, 2006.

KUMAR, B. R.; PRASAD, N.; PRASAD, G.; KUMAR, G. Synthesis, dc conductivity and dielectric studies on double doped strontium bismuth niobate ceramics. **Materials Today: Proceedings**, Elsevier, v. 11, n. 12, p. 1036–1040, 2019.

LONG, S.; MCALLISTER, M.; SHEN, L. The resonant cylindrical dielectric cavity antenna. **IEEE Transactions on Antennas and Propagation**, IEEE, v. 31, n. 3, p. 406–412, 1983.

MCALLISTER, M.; LONG, S. A.; CONWAY, G. Rectangular dielectric resonator antenna. **Electronics letters**, IET, v. 19, n. 6, p. 218–219, 1983.

MOULSON, A. J.; HERBERT, J. M. **Electroceramics: materials, properties, applications**. 1. ed. Chichester, UK: John Wiley & Sons, 2003.

NASCIMENTO, J. do; OLIVEIRA, R.; CARMO, F. do; MORAIS, J. de; SALES, J.; SILVA, M.; GOUVEIA, D.; ANDRADE, H. de; JÚNIOR, I. Q.; SOMBRA, A. Effect of (pr-yb) co-doping on the luminescence and dielectric behaviour of lanbo 4 ceramic. **Journal of Electronic Materials**, Springer, v. 49, n. 10, p. 6016–6023, 2020.

OLIVEIRA, R. G. M.; MORAIS, J. E. V. de; BATISTA, G. S.; SILVA, M. A. S.; GOES, J. C.; SOMBRA, A. S. B. Dielectric characterization of bivo4-tio2 composites and applications in microwave range. **Journal of Alloys and Compounds**, Elsevier, v. 775, n. 1, p. 889–895, 2019.

PETOSA, A. **Dielectric resonator antenna handbook**. 1. ed. Universidade de Michigan: Artech, 2007.

POOLE, C.; DARWAZEH, I. **Microwave active circuit analysis and design**. 1. ed. University College London: Academic Press, 2015. ISBN 978-0-12-407823-9.

POZAR, D. M. **Microwave engineering**. 1. ed. India: John wiley & sons, 2012.

RIETVELD, H. M. A profile refinement method for nuclear and magnetic structures. **Journal of applied Crystallography**, International Union of Crystallography, v. 2, n. 2, p. 65–71, 1969.

SANCHO, E.; SILVA, P.; JÚNIOR, G. P.; RODRIGUES, H.; FREITAS, D.; SOMBRA, A. High dielectric permittivity of srbi$_2$nb$_2$o$_9$ (sbn) added bi$_2$o$_3$ and la$_2$o$_3$. **Journal of Electroceramics**, Springer, v. 30, n. 3, p. 119–128, 2013.

SEBASTIAN, M. T. **Dielectric materials for wireless communication**. 1. ed. India: Elsevier, 2008.

SILVA, M.; FERNANDES, T.; SOMBRA, A. An alternative method for the measurement of the microwave temperature coefficient of resonant frequency (τ f). **Journal of Applied Physics**, American Institute of Physics, v. 112, n. 7, p. 074106, 2012.

SINGH, P.; JHA, R. K.; SINGH, R. K.; SINGH, B. Memory improvement with high-k buffer layer in metal/srbi2nb2o9/al2o3/silicon gate stack for non-volatile memory applications. **Superlattices and Microstructures**, Elsevier, v. 121, n. 1, p. 55–63, 2018.

STUTZMAN, W. L.; THIELE, G. A. **Antenna theory and design**. 3. ed. USA: John Wiley & Sons, 2012. ISBN 978-0-470-57664-9.

WANG, G.; ZHANG, D.; LI, J.; GAN, G.; RAO, Y.; HUANG, X.; YANG, Y.; SHI, L.; LIAO, Y.; LIU, C. et al. Crystal structure, bond energy, raman spectra, and microwave dielectric properties of ti-doped li3mg2nbo6 ceramics. **Journal of the American Ceramic Society**, Wiley Online Library, v. 103, n. 8, p. 4321–4332, 2020.

WEI, T.; JIA, B.; SHEN, L.; ZHAO, C.; WU, L.; ZHANG, B.; TAO, X.; WU, S.; LIANG, Y. Reversible upconversion modulation in new photochromic srbi2nb2o9 based ceramics for optical storage and anti-counterfeiting applications. **Journal of the European Ceramic Society**, Elsevier, v. 40, n. 12, p. 4153–4163, 2020.

WU, J. Bismuth layer structured ferroelectrics. In: **Advances in Lead-Free Piezoelectric Materials**. Singapore: Springer, 2018. p. 379–396.

WU, M.; LOU, X.; LI, T.; LI, J.; WANG, S.; LI, W.; PENG, B.; GOU, G. Ni-doped srbi2nb2o9–perovskite oxides with reduced band gap and stable ferroelectricity for photovoltaic applications. **Journal of Alloys and Compounds**, Elsevier, v. 724, n. 1, p. 1093–1100, 2017.